European Polymer Journal 117 (2019) 208–216

Contents lists available at ScienceDirect

European Polymer Journal

journal homepage: www.elsevier.com/locate/europolj

Structure-morphology impact upon segmental dynamics and diffusion in the biodegradable ultrafine fibers of polyhydroxybutyrate-polylactide blends

Alexey Iordanskii[a,*], Svetlana Karpova[b], Anatoliy Olkhov[a,c], Pavel Borovikov[d], Natalia Kildeeva[e], Yong Liu[f]

[a] Semenov Institute of Chemical Physics, Kosygina 4, Moscow, Russian Federation
[b] Emanuel Institute of Biochemical Physics, Kosygina 4, Moscow, Russian Federation
[c] Plekhanov Russian University of Economics, Stremyanny per. 36, Moscow, Russian Federation
[d] Kulakov National Medical Research Center for Obstetrics, Gynecology and Perinatology, Moscow 117997, Russian Federation
[e] A. Kosygina Russia Gos University, ul. Ordzhonikidze, 13, Moscow, Russian Federation
[f] Beijing Key Laboratory of Advanced Functional Polymer Composites, Beijing University of Chemical Technology, Beijing 100029, China

ARTICLE INFO

Keywords:
Electrospinning
Ultrathin fibers
PHB/PLA fibrillar blends
Water absorption
Drug diffusivity
Drug release
Cylindrical and ellipsoidal geometry

ABSTRACT

An innovative remedies' implementation with a focus on the transition from custom macro- to nano-scaled therapeutic polymer vehicles relies upon the appropriate design of novel drug-polymer compositions, their functionalization at molecular and nano-scale levels, and addressed diffusion-kinetic processes that control drug distribution at any given time in both a proper polymer implant and surrounding biological media. In the framework of this paradigm, ultrathin fibers formed by blending poly(3-R-hydroxybutyrate) [PHB] with poly (L-lactic acid) [PLA] and loaded with modeling drug (dipyridamole [DPD]) were fabricated by solution electrospinning. PHB/PLA ratio and DPD content affected considerably the geometric shape, crystallinity of a single filament. As follows from the optical microscopy and SEM data, in the absence of the drug or at its low concentration (< 3 wt.%), the PHB/PLA fibers appear as ellipsoid-like fragments alternating with cylindrical ones. At the higher content of the drug (3–5%), the abnormal ellipsoid-like structures disappear and all the fibers have cylindrical geometry. By the DSC technique it was shown that PHB/PLA ratio influenced on the crystallinity of fibers and modulated the general course of DSC thermograms. The ESR spectra of the TEMPO radical preliminary embedded into fiber volume represent a superposition of two elementary spectra belonging to the radical populations with different correlation times τ_1 and τ_2 that reflects heterogeneity of the PHB and PLA intercrystalline amorphous regions with slow and fast segmental dynamics respectively. The combination of structure-morphology characteristics of the ultrathin fibers determines the polymer dynamics and drug diffusivity as well as the corresponding profiles of drug release. A coherent model of drug release from the PHB fibrillar and ellipsoidal mats was advanced.

1. Introduction

Homo-polymeric and hybrid vehicles of drugs intended for targeted controlled delivery are widely practiced in the various dosage forms such as the modern therapeutic systems, matrices and templates in tissue engineering, transdermal patches, micro- and nano-sized particles, ultrathin fibers, micelles, etc. [1–5]. Development of innovative remedies includes the appropriate design of novel drug-polymer compositions, their miniaturization at molecular and nano-scale levels, and addressing diffusion-kinetic processes which control drug spatial distribution at any given time in both the proper polymer matrix and surrounding biological media.

One of the most economically and technologically efficient ways to produce ultrathin fibers (UF) and corresponding fibrillar matrices (mates) is the electrospinning (ES) of polymer solutions or melts [6,7]. Among the principal advantages of nanofibrillar vehicles it should be note their high surface/volume ratio that enhances drug absorption capacity and effective biointegration of fibrillar implants [8]. A rather large number of studies have been devoted to the ES production of biodegradable and bioresorbable fibrillar materials where comprehensive and the in-depth analysis of technological conditions is presented, see e.g. [9,10]. This paper considers bio-based and biodegradable polyesters belonging to the families of poly(α-hydroxyacid)s [poly-RL-lactide, **PLA**] and poly(β-hydroxyacid)s [poly(R-3-hydroxybutyrate),

* Corresponding author.
E-mail address: aljordan08@gmail.com (A. Iordanskii).

https://doi.org/10.1016/j.eurpolymj.2019.05.012
Received 13 January 2019; Received in revised form 27 April 2019; Accepted 9 May 2019
Available online 14 May 2019

PHB] which are commonly used in tissue engineering, orthopedic surgery and many other medical devices and therapeutic systems [11,12]. Diversity in their polymer structures and above all in the crystallinity degree determines the variety of mechanical behavior and diffusional transport as well as the rate of macromolecular chain cleavage. It is quite possible that the discrepancy in exploitation behavior for two polyesters of similar chemical structure should be most clearly visible at a submicron level, explicitly for ultrathin fibers. Besides, PHB/PLA composites allow the experts to get a series of novel biodegradable materials, the morphology and dynamics of which can smoothly change during the transition from one composition ratio to another.

Another direction of UF polymer products' exploration includes the extensive group of works that reveal an impact of geometry (diameter), morphology, crystallinity and other structural characteristics upon functional behavior of fibers and mates [13–15]. Against the background of these investigations, encapsulation of drugs under electrospinning conditions affects the structure-morphology features of the fibrils and the mats and hence influences on kinetic characteristics such as segmental mobility, (bio)degradation intensity, diffusivity, and drug release profiles. It is well established that in the performance of macromolecular therapeutic systems drug diffusivity dominates and in combination with polymer swelling, dissolution, hydrolysis, and phase transitions it determines both the variety of addressed mechanisms and diversification of drug spatial-temporal patterns [15,16]. Earlier, the authors have obtained the intrinsic data on drug release from plane films, microspheres, and ultrathin fibers on the base of PHB as one of appropriate biodegradable vehicles of drugs [17–19]. Recently, in our previous work [20] the blends of PHB/PLA in the fibrillar form have been produced by melt electrospinning. Special attention has been paid to the impact of the drug, dipyridomole (DPD), upon geometry, crystallinity, and morphology of the fibrillar excipience; all of them determine the kinetic profile of DPD release and duration of prolongation effect as well. Selection of DPD as a model drug compound was determined by (a) its wide application in therapeutic practice as antihypertensive, anticoagulant remedy, and (b) extended exploration of drug release from films, microparticles, and nanofibers [21,22].

The principal idea of the paper includes the coherent analysis of drug diffusion (DPD) as a dominant impact upon total process of drug release. Here we have used the solution-spun ultrathin fibres on the base of PLA/PHB compositions with different polyester ratios. Additionally the morphological and segmental dynamic characteristics of these biopolymer vehicles have been represented, that could clarify the drug release features in biodegradable therapeutic systems and elucidate the interrelation between fibrillar structure and spatial-temporal pattern in the ultrathin fibrils.

2. Material and methods

2.1. Materials

The PHB was kindly supplied by Biomer Co (Germany), as a lot 16F. The initial polymer was in the form of white powder with particle size of 5–7 μm and $M_W = 2.1 \cdot 10^5$ Da. The PHB powder was evacuated at 60 °C for 4 h in a vacuum oven. PLA particles (Mn = 100 000; Zhejiang Hisun Biomaterials Co., Ltd., China) with average diameter 0.3–0.8 mm were dried at 60 °C for 6 h in a vacuum oven before solution in chloroform. Dipyridamole (DPD) (Mw = 504.63; > 98.0%) was purchased from Beijing Inoke Technology Co. Ltd., China. To prepare the solution for following electrospinning both polyesters were dissolved in chloroform (7% wt.) under stirring at 40 °C at different PHB/PLA ratio: 1/0 (PHB), 9/1, 3/7, 5/5, 7/3, 1/9 and 0/1 (PLA).

2.2. Electrospinning technique

Ultrathin PHB/PLA fibers were produced by solution-mode electrospinning at a voltage of 15 kV using an EFV-1 one capillary laboratory facility (Russia). The distance between two electrodes was 18 cm. The PHB/PLA/DPD solutions in chloroform prepared for electrospinning had dynamic solution viscosity in the interval 2–9 Pa·s measured by a Ubbelohde glass capillary viscometer, specific bulk conductivity of $\sim 10^{-3}\ (\Omega\ m)^{-1}$, volume flow of the forming solution of $10–12 \times 10^{-5}$ g/s. The final dipyridamole (DPD) concentration in the PHB/PLA compositions had values 1, 3, and 5 wt.%. All the polymer solutions were used immediately after preparation. The viscometer was immersed in a constant temperature bath that was controlled at 25 °C within ± 0.2 °C, the effluent times were reproducible to ± 0.5%, and the effluent times were measured with an accuracy of ± 0.05 s.

2.3. Electron paramagnetic resonance

The molecular mobility was studied by the spin probe method on an automated EPR-V spectrometer (Semenov Institute of Chemical Physics, Russian Academy of Sciences). The probe was a stable nitroxide radical 2,2,6,6-tetramethylpiperidine-1-oxyl (TEMPO). The radical was introduced into the fibriles from vapors at a temperature of 60 °C with limited concentration about $3.7 \pm 0.4 \cdot 10^{17}$ spin cm^{-3} that was determined by double integration of ESR spectra. The EPR spectra did not have the saturation feature that was verified with the intensity dependence on the microwave field strength. The correlation times of radical rotation (τ) were calculated from the EPR spectra by the equation [23]

$$\tau = \Delta H^{+}[(I^{+}/I^{-})^{0.5} - 1] \times 6.65 \times 10^{-10}(s) \quad (1)$$

where ΔH^{+} is the width of the spectrum component in a weak field; and I^{+}/I^{-} is the intensity ratio in a weak and strong field, respectively. The measurement error for τ was ± 5%.

2.4. Controlled release rate registration

The DPD release from the PHB/PLA mats was carried out as follows: a rectangular fragment of the mat (~10 mg) was cut out from the electrospun final product and then it was suspended in 50 mL of phosphate buffer medium (pH = 7.4 ± 0.2) at 37 °C under continuous stirring at a moderate speed of 200 rpm in a thermostatically controlled glass flask. To estimate the amount of drug released into aqueous medium, 3 cm^3 of test aliquot was drawn off with the pipette in appropriate time intervals and analyzed by UV–VIS spectrometer DU65 (Beckman Coulter Inc., Ca., USA) at the wavelengths in the interval 295–300 nm. The maximum of UV absorption band for DPD shifted in the given range. To control the displacement of the maximum, the full UV spectrum was measured in every 10 min of controlled release process. Additionally, each experimental kinetic point measurement was accompanied by background optical density recording. For every aliquot removed, the same quantity of fresh water/buffer was added. Each measuring was repeated threefold and the averaged value has been used as one experimental point.

2.5. Instrumental methods

DSC curves' measurements were performed with the fibrillar samples using a TA Instruments model Q20 DSC, New Castle, DE, USA. The mates of ~10 mg weight were cut and crimped in standard Al pans. The DSC cell was purged with nitrogen during measurements (20 mL/min). The samples were equilibrated at 40 °C then ramped up to 180 °C at the rate 10 °C/min and held isothermally for 3 min. After this procedure they were cooled until 0 °C with the same rate 10 °C/min. The melting (Tm) and the glass transition temperatures (Tg) were determined from the peak maximum and the inflection point of the heating scan. Data were analyzed using TA Universal Analysis v4.5A software, New Castle, DE, USA.

To obtain information on the surface morphology of PHB films, SEM

observation was performed with the JSM6510LV JEOL LLC scanning electron microscope (Tokyo, Japan) for samples coated with vapor-deposited gold (Au). The samples were mounted onto an aluminum stud and coated with Ag using a sputter (Polaron E5200, Denton Vacuum, Moorestown, NJ, USA) set at 25 mA for 10 s.

AFM observation was performed on a Ntegra Prima (NT-MDT, Spectrum Instruments. Zelenograd, Russia) directly for uncoated samples. Topographic images of square areas of 18 μm × 18 μm were acquired with micro cantilever CSG01 Spectrum Instruments (Zelenograd Russia) fabricated from low-stress silicon nitride with a spring constant of 0.03 N/m and nominal radius of 10 nm.

2.6. Statistics and data availability statement

The mat thicknesses were equal to 86 ± 4.1 μm with accuracy 0.0434 for all the polymer ratios. Precision has been calculated for all of the experimental points on the kinetic curves in Figs. 5 and 7. It was represented as the relative standard deviation (RSD). for three independent measurements. For the kinetic curves of DPD release (Fig. 7), the RSD values vary in the range 4.5–7.1%. The statistical precision depended on the DPD concentration in the polymers. In the initial concentration range (1 wt.%) the RSD values did not exceed 4.5%, while at higher DPD concentration (3 and 5 wt.%) they increased with the drug concentration until 6.9–7.1%.

The raw processed data required to reproduce these findings cannot be shared at this time due to legal and ethical reasons related to a Mr. P. Borovikov's and phd A. Olkhov dissertations forthcoming approval.

3. Results and discussion

3.1. Optical and AFM microscopy

In considering the microphotographs of the mats (see Fig. 1C and D) formed by the PHB/PLA blends with polyester ratios 7/3 and 3/7 respectively, it was observed disordered accommodation of the fibrils reinforced with numerous entanglements that imparts additional mechanic stability to the network mats. At the same time, it should be noted the appearance of spindle-like morphologies and a subsequent rise of their diameter from 5 to 10 μm for PHB/PLA (3/7) to 15–25 μm for the pristine PLA (0/1). Along with this, by increasing in the diameter of the defects, the more chaotic packing of fibers is observed. Given effect could be related to the relatively low velocity of solvent evaporation from the PLA jet under electrospinning performance that is caused by fairly higher chloroform affinity to PLA as compared with PHB. Actually, the distinction between solubility parameter of chloroform (δ_{ch} = 19 $MPa^{1/2}$) and corresponding thermodynamic characteristics of the polyesters somewhat more for PHB (δ_{PHB} = 20 $MPa^{1/2}$ [24]) than for PLA (δ_{PLA} = 19.0 $MPa^{1/2}$ [25]). The comparative observation of chloroform evaporation (desorption) from PHB and PLA films in Mac-Bain vacuum microbalance experiments has shown that the desorption rate from the former was essentially higher than the analogous characteristic of the latter. Consequently, the PLA fibers exist in viscous and rubbery state for longer time and are affected by disordered thermal motion of polymer molecules. In contrast, the PHB fibers have ability to desorb the solvent fast enough and partial orientation of polymer filaments in the polymer jet does not have appropriate time to be disordered due to the fast solidification of the polyester. So, in the Fig. 1B the well-ordered fiber strands are exposed but they disappeared with the rise of PLA content in the fibrillar blends

To portray the morphology of fiber surfaces the AFM technique has been used. The Fig. 2 shows the 3D images' sequence of the fibers with the various polyester ratios. As seen in the Figure, for the pristine PHB its surface has the local roughness. The similar morphology was found earlier for the PHB films and described in our paper [26].

The AFM images depict that with PHB content decreasing until 5/5 ratio, the averaged cross size does not change practically and keeps the constant value in the range 8.0–8.5 μm. At the transition to the fiber compositions with the PLA predomination, the fiber diameters are markedly increased and approached the supreme value (12 μm) for the pristine PLA. It is appropriate to note that for ultrafine fibers obtained by melt electrospinning of the same pair of polyesters blended, their diameter is increased with PHB concentration [20]. It also follows from AFM findings that solution electrospun fibers are quite closely packed in the mat volume.

As we have just noted, the cause of surface roughness and general unevenness could be the fast evaporation of the solvent and simultaneously the high crystallinity of PHB when the crystalline entities (lamellae and spherulites) have the geometric sizes being comparative with the fiber diameter. Actually, for the next ratios of PHB/PLA blends with the lower content of PHB (Fig. 2C–E) and correspondingly low crystallinity (see Table 1), the surface irregularities are smoothed out, that is, the surface is becoming more uniform. However, here the textured bands directed predominantly along the fiber axes are clearly remarkable and like the above optic data the proper fibers form the tighter packing without spatial orientation. The exception is the 9/1 content where the fibers have the orientation that is supported by the Fig. 2B.

As seen in Fig. 2E, the surface of the pristine PLA fibers is the smoothest one and in a less degree shows any morphological elements and rough structures. The variation of fibrillar packing density in the mat volume should affect the transport characteristics of fiber ensembles, namely the diffusion and absorption of water, solvent evaporation and drug release profiles that will be explored in the following section.

3.2. Thermal characterization of PHB/PLA fibrillar blends.

As a result of blending polyesters, along with evolution of morphology, the changes of thermal and crystalline characteristics of ultrathin fibers should be expected. To study the thermo-physical properties of the fibers, the DSC technique was used. With this object, the DSC heating curves of PHB/PLA fibrillar mats have been depicted in Fig. 3. This figure presents the basic thermal transitions of the constitutive components in the fibers such as melting of crystalline phase,

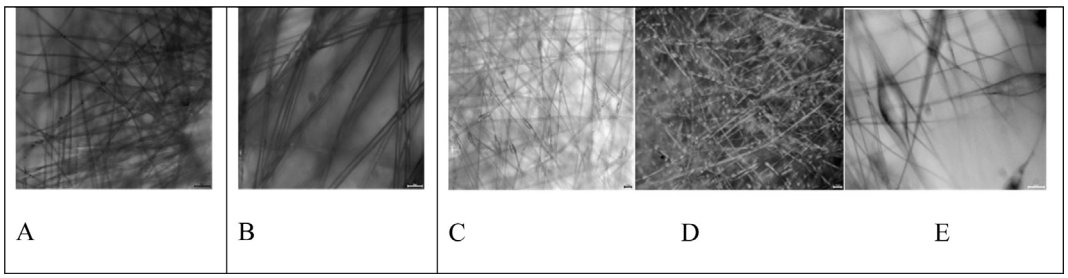

Fig. 1. Optical microphotos of PHB/PLA fibrillar mats at different ratio of polymer components A: 1/0, B: 9/1, C: 7/3, D: 3/7, and E: 0/1 at the same magnification (200X).

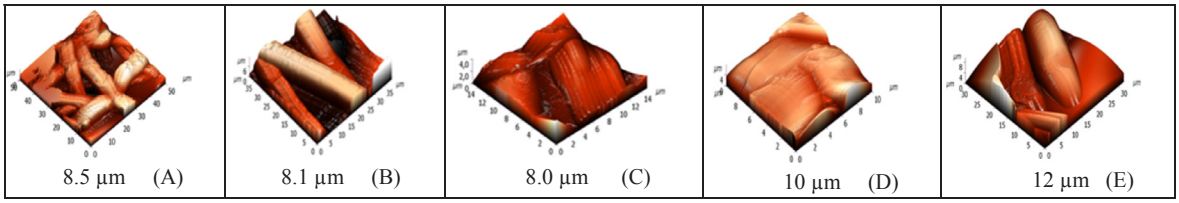

Fig. 2. AFM microphotos of PHB/PLA fibrillar mats at different ratio of polymer components A: 1/0, B: 7/3, C: 5/5, D: 3/7, and E: 0/1. Below the diameters of the fibriles are presented.

Table 1
Thermal characteristics of PHB/PLA ultrathin fibers.

Content PHB/PLA*	T_g	T_m	ΔH_m	T_c	ΔH_c	T_{cc}	ΔH_{cc}	ΔT_{uc}
	°C	°C	J/g	°C	J/g	°C	J/g	°C
1:0 (PHB)	–	177	85.3	114.0	81.2			63
9:1	–	177	77.0	110.5	73.5			66.5
7:3	78.4	172.5	56.3	104.5	49.8			68
5:5	–	174	43.6	103.5	40.0	89.8	21.3	70.6
3:7	–	174.5	37.8	–	–	91.4	20.6	
1:9	57.8	167	32.6	99.5	19.8			67.4
0:1 (PLA)	63.9	169	32.1	100.7	26.0			68.3

**$\Delta T_{uc} \equiv T_m - T_c$ as a difference between melting and crystallization temperatures.
* wt. ratio

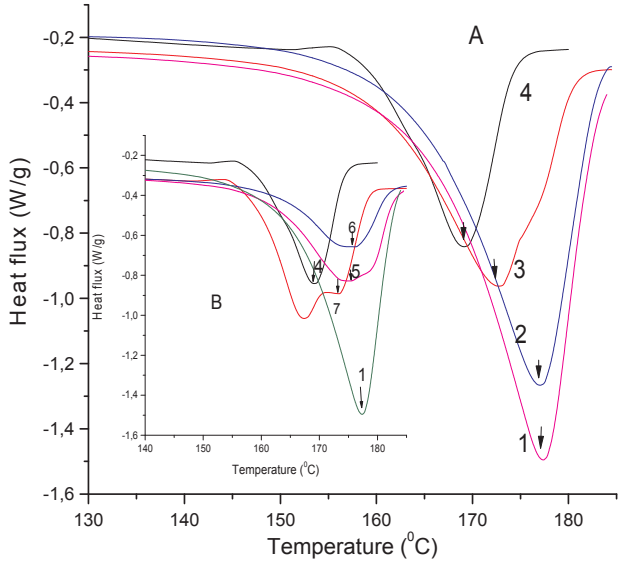

Fig. 3. DSC curves of ultrathin fibers in the field of melting for PHB, PLA, and their blends.PHB/PLA ratio A: PHB (1), 9/1 (2), 7/3 (3), PLA (4); B: 5/5 (5), 3/7 (6), 1/9 (7).

glassy state transition, cold crystallization, and crystallization during the specimens cooling. All the characteristic points and melting enthalpy increments (ΔH_m) are presented in the Table 1.

As it follows from the Table 1, the melting temperatures are monotonically decreased with the addition of PLA from 177 °C for pristine PHB to 169 °C for pristine PLA. In accordance with the difference in crystallinity, the specific melting enthalpy is essentially decreased with the increase of PLA content in the range 85–32 J/g. Both ultimate values of ΔH_m correspond to the melting enthalpy of PHB and PLA respectively. Analogously, the temperature of single point glassy-state transition (T_g) is decreased with growth in the PLA content and clearly identified for the PLA fibers at ≈64 °C. At a high content of PHB in the system, the glassy-state transition was not observed on the DSC curves. The analogous effect of T_g vanishing was noticed for the PHB and PHB/PLA films that could be interpreted by high crystallinity PHB which masks the glassy-state transition registration. For the blend fibers with a moderate content of PHB (5/5, 3/7), the temperature of cold crystallization (T_{cc}) is clearly observed. Both samples give approximately the same values of Tcc and corresponding enthalpy of crystallization. This effect should be taken into account at calculation the total values of crystallinity.

At the regime of DSC after 1st scan heating, the following cooling demonstrates the appearance of the exothermic single peak reflecting the fibrile melt crystallization in the range 114–100 °C. As in the event of fibrils' melting, the temperature of crystallization monotonically decreased with PLA content, so that the undercooling range [25], namely the difference between temperatures of melting and crystallization ($\Delta T_{uc} \equiv T_m - T_c$), remains approximately constant for all the blends. The span of ΔT_{uc} reflects the temperature diapason of metastable overcooled state of the samples, which is wider than that for pristine PHB because of intermolecular interaction in the fibers.

3.3. Dynamics of ESR probe in the PHB/PLA fibers

For crystalline bio-based polymers such as PHB and PLA, segmental dynamics in amorphous phase is essentially determined by their crystallinity degree. In ultrafine fibers, as the sequence of spatial confinements, a conformational set of macromolecules is scantier relative to the macro-objects such as films, slabs, conventional medical implants, and etc. Therefore, in a nano-sized confined fibrillar volume the segmental mobility in inter-crystalline fields should be affected by crystalline fraction more strongly than in the macro- and micro-sized specimens. The previous section was devoted to thermal analysis of DSC curves for PHB/PLA fibers where it was shown that PHB content increment leads to the crystallinity increase and therefore to a change the inherent structure and the total size of amorphous phase.

Segmental dynamics of polyester molecules in PHB/PLA fibrils and in corresponding mats can be efficiently investigated by probe ESR technique. This methodical approach was widely accepted for the macro-sized objects' study and particularly for the PHB/PLA films with the similar polyester ratio [27]. As in the films, the ESR spectra of TEMPO encapsulated in the fibers with the same polyester ratio have the composite form (see Fig. 4) that determines the superposition of two single spectra. The both spectra reflect the rotational dynamics of two populations of radicals with the characteristic correlation times, τ_1 and τ_2. Here τ_1 corresponds to slow frequency of radical rotation in relatively denser fields of amorphous phase while τ_2 does the high rotation of radical encapsulated in less dense fields of amorphous phase of the fibers.

In the Fig. 5A the τ_2 dependence on the polyester ratio of the fibrils is depicted. This dependence is nonlinear and has a gently sloping minimum in the wide ratio range, 10–70% PHB. Consequently, in the blend fibrils with polyester ratio 3/7, 5/5 and 7/3 the amorphous areas formed by a rather loose packaging of macromolecules with high segmental mobility as evidenced by low correlation time values. The presented rotation dynamics of the stable radical in fibrillar blends correspond well with the analogous dependence of radical rotation activation energy (E_a), as it is shown in Fig. 5B. There is a well-pronounced minimum which is indicative of the activation barrier decrease

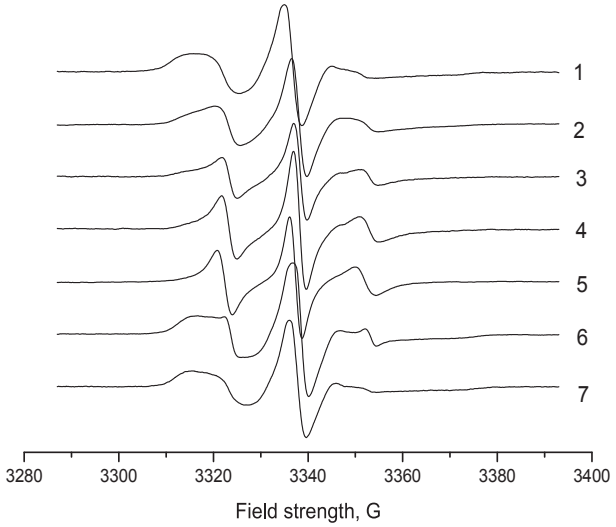

Fig. 4. The ESR spectra of nitroxide radical (TEMPO) encapsulated in the PHB/PLA fibers at different polyester ratios: 1 – 1/0 (PHB), 2 – 9/1 3 – 7/3, 4 – 5/5, 5 – 3/7, 6 – 1/9, 7 – 0/1 (PLA). The spectra 2–6 are shifted for the sake of clarity of images thence the axis "y" with arbitrary units is omitted.

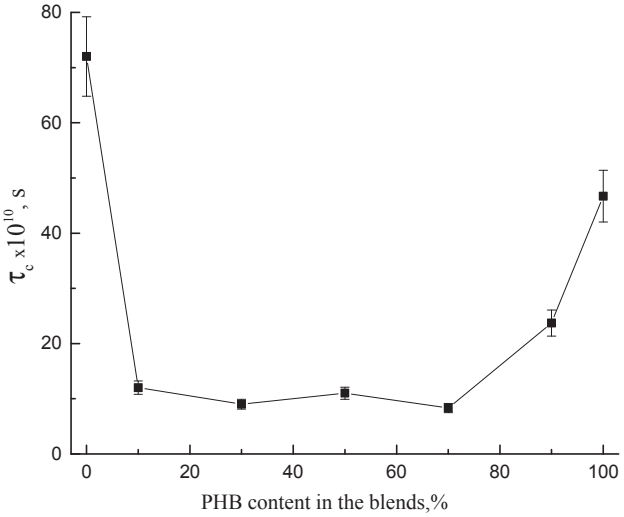

Fig. 5. Dependence of correlation time on the PHB concentration (wt.%) in the PHB/PLA electrospun fibers.

in radical rotation because of decrement crystallinity.

3.4. Water absorption in the PHB/PLA mats.

The water absorption in polymer fibrillar mats follows as a consequence of three distinct processes, namely the external water transport in inter-fibrillar voids (pores), following its dissolution in surface fibrillar layer, and final stage including diffusion into the bulk of fibrils. The ultimate amount of absorbed water in the mats results from its intra-fibrillar thermodynamic solubility and water retained in the inter-fibrillar voids. Water molecular solubility depends on the content of polar polymer groups (its hydrophilicity), their chemical nature, and polymer crystallinity. The last factor determines mainly the free volume for the allocation of water molecules. The hydrophilicity of the fibers is the key factor of ultimate water amount but the free volume formed by the segmental mobility (see the previous section) affects solubility quite week and does rather the water diffusivity.

In the Fig. 6 the water vapor absorption isotherms are presented for the fibrillar samples with different ratio of the polyesters (PHB/PLA).

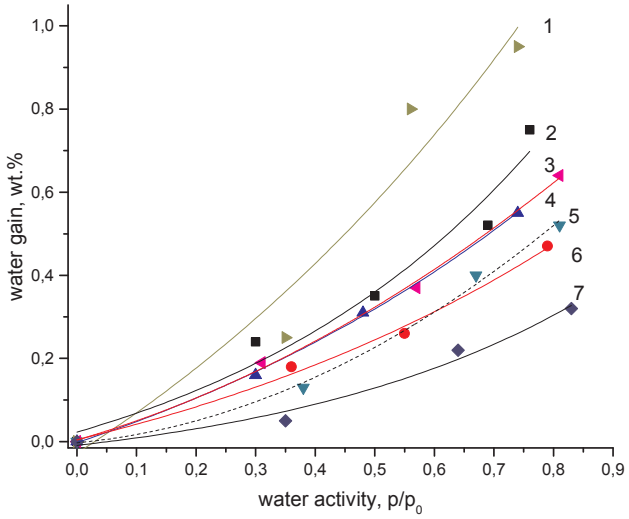

Fig. 6. Isotherms of water vapor absorption for PHB/PLA blend fibers at 25 °C. 1 (PLA), 2 (9/1), 3 (3/7), 4 (5/5), 5 (7/3), 6 (9/1), 7 (PHB).

Relatively far from the point of water condensation in the inter-fibrillar voids, at water vapor activity $p/p_0 < 0.8$, the proper sorption in fiber volume plays a primary role in the total water absorption. This thesis is confirmed by the low values of absorbed water ($C_w < 1.0$ wt.%) which are typical for the corresponding nonporous films of the same polyesters. In contradistinction to liquid water absorption by the fibrillar mats at $p/p_0 = 1$, when the dominant quantity of water was absorbed in the voids (see the Fig. 2. in [28]), the vapor absorption has predominantly occurred in the very fibers and therefore is sensitive to chemical nature and crystallinity of PHB/PLA blends. As it follows from the Table 1, the PHB crystallinity degree is significantly larger than the PLA one. Hence, the water solubility in low crystalline PLA has the maximal value of water absorption, high crystalline PHB has the minimal characteristic, and the blended fibrillar systems with different occupy the intermediate positions in accordance with corresponding PHA/PLA ratios.

The appearance of all absorption isotherms resembles the BET isotherms that are typical for the uptake in polymer systems with relatively weak polarity if the energy of interaction among sorbate molecules exceeds the energy of sorbate - polymer interaction; in other words the "water - water" interaction dominates "water - ester group" interplay. The BET modeling formalism implies that surface polycondensation of several layers of sorbate, but in our case the water clustering in the fibrillar volume is more likely. The final decision to this dilemma should be performed after additional experimental providing e.g. by thermo-mechanical testing to determine the presence of water plasticizing effect in the fibers. However, the additional argument supporting the water penetration into the polymer bulk has been presented in our previous work [29] where it was shown that the interaction of water molecules with functional groups of PHB occurred in whole volume of samples and this effect depressed the water transport in the polymer volume.

3.5. Diffusion in fibers of ellipsoid and cylindrical geometry

Most natural and synthetically fabricated granular polymer systems often contain ellipsoid-like particles whom geometry affects absorption and diffusion behavior of the heterogeneous materials. Micro-ellipsoidal entities are commonly encountered in chemical engineering, nature, agriculture, pharmaceutical products and in the other areas of human endeavor [30–32]. The comprehension of diffusion modeling in a fibrous matrix requires the structure-morphology description including the complex geometry of ultrathin fibers. As it was depicted in

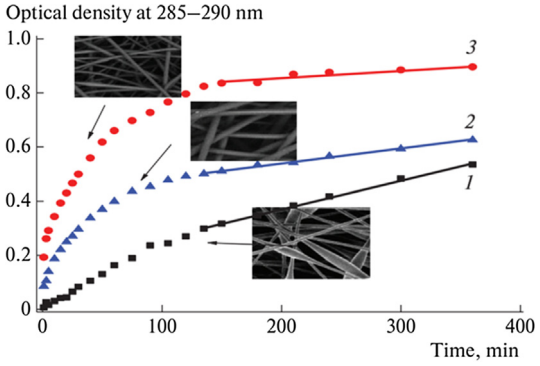

Fig. 7. Typical kinetic profiles of DPD controlled release from PHB fibres. DPD concentrations are (1) 1, (2) 3, and (3) 5 wt.%. Micrographs illustrate the shape of fibres (×1000).

the previous SEM microphotographs, the PHB/PLA mats present the randomly oriented fibrillar cylinders in the combination with the ellipsoidal elements that are distributed randomly in 3D fibrillar space. It is worth to note that the PHB/PLA mats are the moderately rigid matrices where filament orientation and interfibrillar spacing are maintained by weak non-covalent interactions and the physical knots (entanglements). In principal, fiber displacement in such systems can occur as a result of applied mechanical force, thermal fluctuation, and solvent absorption. Simultaneously, the network morphology could be depicted as a fibrous mesh, with the space between the fibers forming voids (or 'pores') through which an initially embedded drug can move off. The volume fraction occupied by the ultrathin fibers confines the drug diffusion space, the geometry of which directly affects rate of drug transport. The relationship between solute diameter, $2r_s$, and pore diameter, $2r_a$, should be factored into drug release model that regards the electrospun mat as the molecular-sieve with a relevant selectivity.

The Fig. 7 displays the DPD release profiles from the PLLA/PHB ultrathin fibres that are assembled in the mats in the process of solution electrospinning (SES). The small displacement in DPD maximum in UV spectrum is likely caused by desorption of the PHB oligomer residues from bulk of fibers into recipient solution and following UV-light scattering. In comparison to the fibrillar mats obtained by melt electrospinning recently [20], for the SES fibres the drug release profiles have the similar forms. Fibrillar blends of bio-based polyesters demonstrate two specific ranges of the release profiles namely nonlinear and linear ranges, the physical meaning of which has been recently analyzed for both the melt electrospun mats [33] and the solution-cast films with the same PHB/PLA ratio[17].

In concordance with the previously suggested diffusion-kinetic model [28], the initial nonlinear range of the release profiles represents principally the drug diffusion process, while the following linear range corresponds to the superficial hydrolysis of polyester fibres with the adequate loss of polymer weight. As a result of zero-order hydrolytic reaction, the immobilized fraction of the encapsulated drug releases from the cylindrical and ellipsoidal fragments of fibres and from fibrillar mat as the whole system at a constant rate. Thus, during a short term release, the drug concentration in a surrounding aqueous medium (specifically in phosphate buffer) is the sum of the mobile fraction transported via diffusion mechanism and the immobilized fraction released via a zero-order hydrolysis.

In the PLA/PHB fibrillar mat prepared as the rectangular slab that consists of disordered entangled fibres and inter-fibrillar space, the effective drug diffusivity, D_{eff}, is determined by two consecutive processes such as diffusion in the inherent fibre volume with diffusivity (D_f) and the diffusion transport in the inter-fibrillar voids of the mat that are filled by an aqueous solvent (D_W). Describing the two-stage diffusion as the drug transport in the quasi two-layer medium with two different diffusion coefficients, in accordance with the Crank's simplification [34], D_{eff} can be presented as

$$\frac{L_M}{D_{eff}} = \frac{R_f}{D_f} + \frac{L_W}{D_W} \tag{2}$$

where R_f, L_w, and L_M are the averaged geometric characteristics of drug diffusion path in the fibres, the interfibrous voids, and the effective thickness of mats correspondingly. Taking into account the both impacts related to diffusion in cylindrical fibres and ellipsoidal entities simultaneously and the constant drug diffusivity (D_f), the Eq. (2) should be given in the following form

$$\frac{L_M}{D_{eff}} = \frac{R_C R_E}{D_f (R_C + R_E)} + \frac{L_W}{D_W} \tag{3}$$

here R_C and R_E are spatial characteristics of cylindrical fibres and rotational ellipsoids respectively.

The differential equation of diffusion in the cylindrical fiber loaded by uniformly distributed drug has advanced by Crank [34]:

$$\partial C_D/\partial t = (1/r) D_f [\partial(r \partial C_D/\partial r)/\partial r] \tag{4}$$

which is rightfully in the interval $0 < r < R_C/2$, where r is the coordinate of the radial diffusion; symbol C_D denotes the concentration of the drug mobile fraction in the cylindrical fiber with the corresponding constant diffusion coefficient D_f and R_C is the average diameter of the fibers.

In accordance with the in-depth review of J. Siepmann and F. Siepmann [35], the simplified solution of differential Eq. (4) with corresponding initial and boundary conditions makes it possible to obtain the dependence of the cumulative amount of the drug on the time of release from cylindrical fibres (t):

$$M_t = 4\alpha_{ce}[D_f/\pi R_f^2]^{1/2} M_\infty t^{1/2} - \alpha_{ce}[2D_f/R_f^2] M_\infty t \tag{5}$$

where M_∞ is the limiting value of M_t under the infinite time and α_{ce} is the volume portion of cylindrical fibrils relative to the total volume of the fibrils.

Modeling of drug release from a rotatory ellipsoid entity through its constant surface was performed by diffusion equations in prolate spheroidal coordinates. The transition from Cartesian {x,y,z} to spheroidal coordinates {r,θ,φ} was carried out using the following transformations [36]:

$$x = a \cdot \sinh(r) \cdot \sin(\theta) \cdot \cos(\varphi), \tag{6a}$$

$$y = a \cdot \sinh(r) \cdot \sin(\theta) \cdot \sin(\varphi), \tag{6b}$$

$$z = a \cdot \cosh(r) \cdot \cos(\theta), \tag{6c}$$

where r is a positive real number $0 \le r < +\infty$, and $0 \le \theta \le \pi$. The azimuthal angle φ belongs to the interval $0 \le \varphi < 2\pi$, and a is the distance between two focuses of the ellipsoid i.e. focal length, $0 < \le L < +\infty$.

In this scaled system of coordinate, the description of the surface splits between two geometries such as the confocal ellipsoid and the confocal hyperboloid of revolution. The average drug content in the ellipsoidal element with volume V is expressed as follows:

$$\hat{\bar{M}} = \frac{1}{V} \int_V M dV \tag{7}$$

and the mass of released drug, ΔM, at given moment t is equal to

$$\Delta M = M_O - \frac{1}{V} \int_V M dV \tag{8}$$

where M_0 is the initially loaded content of the drug.

In the selected spheroid coordinates, the ΔM dependence on time can be presented with the volume integral and Jacobian ⟨J⟩ as follows

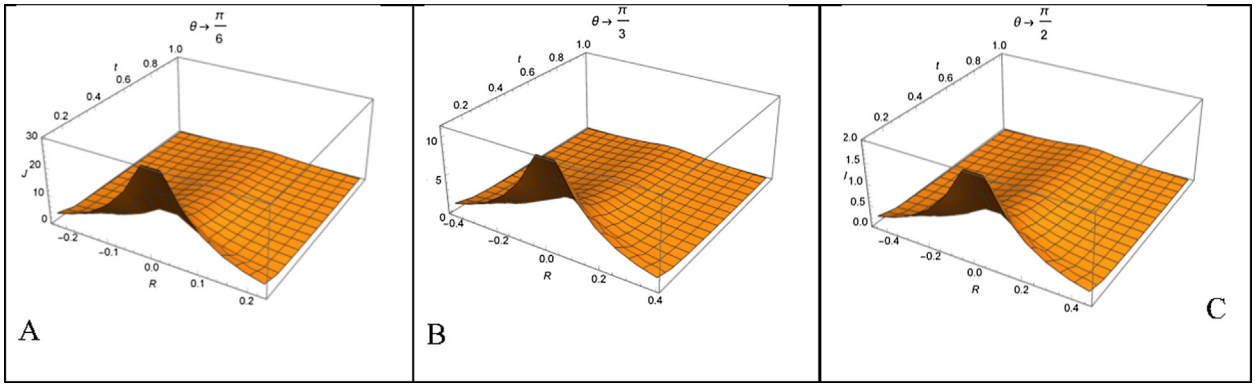

Fig. 8. Drug release flux profiles for the ellipsoid at the different prolate spheroid coordinate (θ): π/6 (A), π/3 (B), and π/2 (C).

$$\Delta M(t) = \int_V C_e(r, \theta, \varphi, t)\langle J\rangle dV = \int_0^R \int_0^{\pi} \int_{-\pi}^{\pi} C_e(r, \theta, \varphi, t)a^3\sin(\theta)\sinh(r)[\sin(\theta)^2 + \sinh(r)^2]d\varphi d\theta d r \quad (9)$$

and providing the separation of variables [34] we have

$$\Delta M(t) = K\exp(-D^2\mu^2 t), \quad (10)$$

where

$$K = \int_0^R \int_0^{\pi} \int_{-\pi}^{\pi} C_e(r, \theta, \varphi, t)a^3\sin(\theta)\sinh(r)[\sin(\theta)^2 + \sinh(r)^2]d\varphi d\theta d r \quad (11)$$

Because of the transcendence of spheroidal functions [37,38], this integral has been calculated only numerically using the programming package Mathematica[TR][39].

Fig. 8 shows the series of drug fluxes at different position of the ellipsoid surface as function of the coordinate and time of release. Based on the calculations in accordance with Eq. (11), the decrease in the angle θ (from π/2 to π/6) leads to the surface curvature increment and simultaneously increasing the drug flux.

Considering the Fig. 8, it is easy to see that the largest ellipsoid fraction belongs to the fibrillar sample with the lowest content of DPD. Hence, the impact of release from ellipsoid-like entities should be maximal.

In view of the foregoing, drug release from the fibers with the cylindrical and spindle-like (ellipsoidal) elements is determined by two kinetic constituents. The latter include drug diffusion in the volume of cylindrical elements described by Eq. (4) and diffusion in the spindle-like elements with geometrical form that is approximated by revolving ellipsoid (see Eq. (10)). Providing a minor contribution of PHB/PLA hydrolysis into general release process, i.e. at relatively small duration of the drug release (short-term of drug release [20]), the total diffusion flux consists of two relevant contributions such as desorption from cylinders and ellipsoidal particles simultaneously:

$$K = \int_0^R \int_0^{\pi} \int_{-\pi}^{\pi} C_e(r, \theta, \varphi, t)a^3\sin(\theta)\sinh(r)[\sin(\theta)^2 + \sinh(r)^2]d\varphi d\theta d r \quad (12)$$

The submitted results argued that the ellipsoid elements being included in the PHB/PLA fibrils can play a prominent role in the control of DPD release owing to its diffusion. The initial release stage followed Fickian kinetic mechanism (classical Case I kinetics), but in the final stage this mechanism was replaced by another process related to the hydrolytic reaction. As in our previous works [17,20,28], the hydrolysis of polyester groups is described by the equation of zero power that is well confirmed by the appearance of the curves in Fig. 7. Additionally, this is expressed by the values of diffusion coefficients and corresponding reaction constants presented in the Table 2.

The DPD loading above 1 wt.% sharply reduces the ellipsoids' formation that confirmed by the Fig. 7 and at following concentrations 3 and 5 wt.% in the PHB/PLA mats the cylindrical fibrils prevail only. In general case, the volume ratio between the cylinders and ellipsoids as the geometric forms of fibrils determines the kinetic profiles of drug release at the initial diffusion stage and does not affect the non-topological chemical process that does not depend on the geometry (the spatial coordinates) of the fibrils.

Table 2
Effective diffusivities (D_f) of DPD controlled release from PHB/PLA fibrils.

PHB/PLA wt. ratio	DPD wt.%	α_{ce}	D_f10^{11}, cm^2/s	R_f10^4, cm
5:5	1	0.45	3.4	4.3
5:5	3	0.90	4.1	2.0
5:5	5	1.00	6.1	0.8
1:0	1	0.35	2.4	4.0
1:0	3	0.85	3.9	1.1
1:0	5	0.95	5.4	0.65

α_{ce} is the volume fraction of cylinders relative to total volume of fibrils.

4. Conclusions

Drug diffusion models have been used by many authors [40–43] to designate the drug release and concomitant processes such as swelling, dissolution, and degradation, which take place in biodegradable therapeutic systems [44,45]. The advantages of transport modeling in comparison with simplified approximations and empirical approaches are that analytical and computer simulations enable the experts not only to predict the kinetic release profile evolution but also to outline the spatial pattern of drug distribution in a therapeutic vehicle, drug front moving, and an aqueous solvent flux that could promote degradation and swelling.

In the many papers which used diffusivity modeling, it was shown that the geometry of polymer vehicles affects crucially the release profiles. Most often computing or analytical solutions were performed for relatively simple geometries such as plane membranes, cylinders, and spheres [46–48] but transport phenomena description in ellipsoid entity types is found extremely rare. A few works have been devoted to moisture desorption from prolate/oblate spheroids as the models of banana or food grains [49,50]. In the case of drug release from ultrathin fibers with the geometry of alternating cylinders and ellipses, the authors could not discovered any scientific publications. Nevertheless, this situation is quite typical in the case of biomedical investigations especially during scaffold exploration or vascular stenting and embolization.

For the series of PHB/PLA fibers, the first-presented kinetic data have been accompanied by structure-morphology features in combination with thermal characteristics. The latter characterize the physical state of the ultrathin fibers and their crystallinity degree that

satisfactory correlate with segmental mobility in the specimens. The multifactor investigation of PLA/PHB ultrathin fibers with the different geometrical forms will allow the experts to facilitate an understanding of operation perspectives in submicron-sized drug delivery vehicles.

Acknowledgements

The paper was financially supported by the RF State Program of Fundamental Scientific Investigation RAN: AAAA-A17-117040610309-0 and the RFBR Science Foundation of Russia (Grant Numbers:18-29-05017 and 18-29-17059) as well as the National Natural Science Foundation of China (Grant Number 21374008). The authors gratefully acknowledge Dr. U. Haenggi and Biomer Co (Krailing, Germany) for kind supplying with PHB and Dr. E. Kucherenko (ICP Moscow) for a drug release experimental support.

Appendix A. Supplementary material

Supplementary data to this article can be found online at https://doi.org/10.1016/j.eurpolymj.2019.05.012.

References

[1] A.H. Blaesi, N. Saka, Fibrous dosage forms by wet 3D-micro-patterning: process design, manufacture, and drug release rate, Eur. J. Pharm. Biopharm. 130 (2018) 345–358, https://doi.org/10.1016/j.ejpb.2018.06.015.
[2] R.A. Perez, H.-W. Kim, Core–shell designed scaffolds for drug delivery and tissue engineering, Acta Biomater. 21 (2015) 2–19, https://doi.org/10.1016/j.actbio.2015.03.013.
[3] C.R. Reshmi, P.S. Suja, T. Subija, A. Sujith, "Nano in micro" architecture composite membranes for controlled drug delivery, Appl. Clay Sci. 166 (2018) 262–275, https://doi.org/10.1016/j.clay.2018.08.015.
[4] Arora, M.R. Prausnitz, S. Mitragotri, Micro-scale devices for transdermal drug delivery, Int. J. Pharm. 364 (2) (2008) 227–236, https://doi.org/10.1016/j.ijpharm.2008.08.032.
[5] Ding, Z. Li, A review of drug release mechanisms from nanocarrier systems, Mater. Sci. Eng., C 76 (2017) 1440–1453, https://doi.org/10.1016/j.msec.2017.03.130.
[6] T.D. Brown, P.D. Dalton, D.W. Hutmacher, Melt electrospinning today: an opportune time for an emerging polymer process, Prog. Polym. Sci. 56 (2016) 116–166, https://doi.org/10.1016/j.progpolymsci.2016.01.001.
[7] X. Hu, S. Liu, G. Zhou, Y. Huang, X. Jing, Electrospinning of polymeric nanofibers for drug delivery applications, J. Control. Release 185 (2014) 12–21, https://doi.org/10.1016/j.jconrel.2014.04.018.
[8] Scott A. Sell, Michael J. McClure, Koyal Garg, Patricia S. Wolfe, Gary L. Bowlin, Electrospinning of collagen/biopolymers for regenerative medicine and cardiovascular tissue engineering, Adv. Drug Deliv. Rev. 61 (12) (2009) 1007–1019, https://doi.org/10.1016/j.addr.2009.07.012.
[9] A. Rogina, Electrospinning process: Versatile preparation method for biodegradable and natural polymers and biocomposite systems applied in tissue engineering and drug delivery, Appl. Surf. Sci. 296 (2014) 221–230, https://doi.org/10.1016/j.apsusc.2014.01.098.
[10] D. Kai, S.S. Liow, X.J. Loh, Biodegradable polymers for electrospinning: towards biomedical applications, Mater. Sci. Eng., C 45 (2014) 659–670, https://doi.org/10.1016/j.msec.2014.04.051.
[11] P. Saini, M. Arora, M.N.V. Ravi Kumar, Poly(lactic acid) blends in biomedical applications, Adv. Drug Deliv. Rev. 107 (2016) (2016) 47–59, https://doi.org/10.1016/j.addr.2016.06.014.
[12] Q. Wu, Y. Wang, G.-Q. Chen, Medical Application of Microbial Biopolyesters Polyhydroxyalkanoates. Artificial Cells, Blood Substitutes, and Biotechnology vol. 37, (2009) 1–12.
[13] F. Acevedo, P. Villegas, V. Urtuvia, J. Hermosilla, R. Navia, M. Seeger, Bacterial polyhydroxybutyrate for electrospun fiber production, Int. J. Biol. Macromol. 106 (2018) 692–697 https://ac.els-cdn.com/S0141813017314113/dx.doi.org/10.1016/j.ijbiomac.2017.08.066.
[14] R. Stepanyan, A.V. Subbotin, L. Cuperus, P. Boonen, M. Dorschu, F. Oosterlinck, M.J.H. Bulters, Nanofiber diameter in electrospinning of polymer solutions: model and experiment, Polymer 97 (2016) 428–439, https://doi.org/10.1016/j.polymer.2016.05.045.
[15] R. Scaffaro, F. Lopresti, Processing, structure, property relationships and release kinetics of electrospun PLA/Carvacrol membranes, Eur. Polym. J. 100 (2018) 165–171, https://doi.org/10.1016/j.eurpolymj.2018.01.035.
[16] M.C. Bottino, V. Thomas, G.M. Janowski, A novel spatially designed and functionally graded electrospun membrane for periodontal regeneration, Acta Biomater. 7 (1) (2011) 216–224, https://doi.org/10.1016/j.actbio.2010.08.019.
[17] E.L. Ivantsova, R.Yu. Kosenko, A.L. Iordanskii, S.Z. Rogovina, E.V. Prut, A.G. Filatova, K.Z. Gumargalieva, S.P. Novikova, A.A. Berlin, Structure and prolonged transport in a biodegradable poly(R-3-hydroxybutyrate)–drug system, Polym. Sci., Ser. A 54 (2) (2012) 87–93, https://doi.org/10.1134/S0965545X12020058.
[18] A.P. Bonartsev, V.A. Livshits, T.A. Makhina, V.L. Myshkina, G.A. Bonartseva, A.L. Iordanskii, Controlled release profiles of dipyridamole from biodegradable microspheres on the base of poly(3-hydroxybutyrate). eXPRESS, Polym. Lett. 1 (12) (2007) 797–803, https://doi.org/10.3144/expresspolymlett.2007.110.
[19] S.G. Karpova, A.A. Olkhov, N.G. Shilkina, et al., Influence of drug on the structure and segmental mobility of poly(3-hydroxybutyrate) ultrafine fibers, Polym Sci. Ser A. 59 (1) (2017) 58–66, https://doi.org/10.1134/S0965545X17010060.
[20] K. Cao, Y. Liu, A.A. Olkhov, V. Siracusa, A.L. Iordanskii, PLLA-PHB fiber membranes obtained by solvent-free electrospinning for short-time drug delivery, Drug Deliv. Trans. Res. 8 (1) (2018) 291–302, https://doi.org/10.1007/s13346-017-0463-7.
[21] P. Punnakitikashem, D. Truong, J.U. Menon, K.T. Nguyen, Y. Hong, Electrospun biodegradable elastic polyurethane scaffolds with dipyridamole release for small diameter vascular grafts, Acta Biomater. 10 (11) (2014) 4618–4628, https://doi.org/10.1016/j.actbio.2014.07.031.
[22] M. Esfandyari-Manesh, M. Javanbakht, F. Atyabi, A. Mohammadi, R. Dinarvand, Dipyridamole recognition and controlled release by uniformly sized molecularly imprinted nanospheres, Mater. Sci. Eng. C31 (8) (2011) 1692–1699, https://doi.org/10.1016/j.msec.2011.07.019.
[23] V.P. Timofeev, A.Y. Misharin, Y.V. Tkachev, Simulation of EPR spectra of the radical TEMPO in water-lipid systems in different microwave ranges, Biophysics 56 (3) (2011) 420–432.
[24] M.P. Arrieta, J. López, D. López, J.M. Kenny, L. Peponi, Development of flexible materials based on plasticized electrospun PLA–PHB blends: structural, thermal, mechanical and disintegration properties, Europian Polym. J. 73 (2015) 433–446, https://doi.org/10.1016/j.eurpolymj.2015.10.036.
[25] R. Auras, B. Harte, S. Selke, An overview of polylactides as packaging materials, Macromol. Biosci. 4 (9) (2004) 835–864, https://doi.org/10.1002/mabi.200400043.
[26] A. Sato, T. Sasaki, Cooperativity of dynamics in supercooled polymeric materials and its temperature dependence predicted from a surface controlled model, Eur. Polym. J. 99 (2018) 485–494, https://doi.org/10.1016/j.eurpolymj.2018.01.003.
[27] Y. Liu, K. Cao, S. Karpova, A. Olkhov, A. Filatova, A. Zhulkina, A. Burkov, S.V. Fomin, D.S. Rosa, A.L. Iordanskii, Comparative characterization of melt electrospun fibers and films based on PLA-PHB blends: diffusion, drug release, and structural features, Macromolecular Symposia 381 (1) (2018) 1800130, https://doi.org/10.1002/masy.201800130.
[28] A.L. Iordanskii, A.A. Ol'khov, S.G. Karpova, E.L. Kucherenko, R.Yu Kosenko, S.Z. Rogovina, A.E. Chalykh, A.A. Berlin, Influence of the structure and morphology of ultrathin poly(3-hydroxybutyrate) fibers on the diffusion kinetics and transport of drugs, Polym. Sci. Ser. A 59 (3) (2017) 343–353, https://doi.org/10.1134/S0965545 X17030075.
[29] A.L. Iordanskii, P.P. Kamaev, G.E. Zaikov, Immobilization influence on water sorption and diffusion in poly(3-hydroxybutyrate), J. Apple Polym. Sci. 73 (1999) 981–985, https://doi.org/10.1002/(SICI)1097-4628(19990808)73:6<981::AID-APP16>3.0.CO;2-Y.
[30] H.M. Jaeger, S.R. Nagel, R.P. Behringer, Granular solids, liquids, and gases, Rev. Mod. Phys. 68 (4) (1996) 1259–1276, https://doi.org/10.1103/RevModPhys. 68.1259.
[31] Y. You, Y. Zhao, Discrete element modelling of ellipsoidal particles using super-ellipsoids and multi-spheres: a comparative study, Powder Technol. 331 (2018) 179–191, https://doi.org/10.1016/j.powtec.2018.03.017.
[32] J. Rong, F. Qiu, T. Zhang, X. Zhang, Y. Zhu, J. Xu, D. Yang, Y. Dai, A facile strategy toward 3D hydrophobic composite resin network decorated with biological ellipsoidal structure rapeseed flower carbon for enhanced oils and organic solvents selective absorption, Chem. Eng. J. 322 (2017) 397–407, https://doi.org/10.1016/j.cej.2017.04.049.
[33] Y. Liu, K. Cao, S. Karpova, A. Olkhov, A. Filatova, A. Zhulkina, A. Burkov, S.V. Fomin, D.S. Rosa, A.L. Iordanskii, Comparative Characterization of Melt Electrospun Fibers and Films Based on PLA-PHB Blends: Diffusion, Drug Release, and Structural Features. Macromolecular Symposia, vol. 381, no. 1. https://doi.org/10.1002/masy.201800130.
[34] J. Crank, The Mathematics of Diffusion, third ed., Clarendon Press, Oxford, 1992.
[35] J. Siepmann, F. Siepmann, Mathematical modeling of drug delivery, Int. J. Pharm. 364 (2) (2008) 328–343, https://doi.org/10.1016/j.ijpharm.2008.09.004.
[36] Y. Mou, J.M. Howe, Diffusion field associated with prolate spheroids in size and shape coarsening, Acta Mater. 45 (2) (1997) 823–835, https://doi.org/10.1016/S1359-6454(96)00201-7.
[37] P. Kirby, Calculation of spheroidal wave functions, Comput. Phys. Commun. 175 (7) (2006) 465–472, https://doi.org/10.1016/j.cpc.2006.06.006.
[38] P.E. Falloon, P.C. Abbott, J.B. Wang, Theory and computation of spheroidal wave functions, J. Phys. A: Math. Gen. 36 (20) (2003) 5477–5495, https://doi.org/10.1088/0305-4470/36/20/309.
[39] E.W. Weisstein, "Spheroid." From MathWorld–A Wolfram Web Resource. http://mathworld.wolfram.com/Spheroid.html.
[40] J. Siepmann, F. Siepmann, Mathematical modeling of drug release from lipid dosage forms, Int. J. Pharm. 418 (1) (2011) 42–53, https://doi.org/10.1016/j.ijpharm.2011.07.015.
[41] B. Narasimhan, Mathematical models describing polymer dissolution: consequences for drug delivery, Adv. Drug Deliv. Rev. 48 (2001) 195–210.
[42] A.C. Balazs, D.F. Calef, J.M. Deutch, R.A. Siegel, R. Langer, The role of polymer matrix structure and interparticle interactions in diffusion-limited drug release, Biophys. J. 47 (1) (1985) 97–104.
[43] J.A. Ferreira, M. Grassi, E. Gudiño, P. de Oliveira, A 3D model for mechanistic control of drug release, SIAM J. Appl. Math. 74 (3) (2014) 620–633, https://doi.org/10.1137/130930674.
[44] E. Kaunisto, M. Marucci, P. Borgquist, A. Axelsson, Mechanistic modelling of drug

release from polymer-coated and swelling and dissolving polymer matrix systems, Int. J. Pharm. 418 (1) (2011) 54–77, https://doi.org/10.1016/j.ijpharm.2011.01.021.
[45] J. Siepmann, A. Göpferich, Mathematical modeling of bioerodible, polymeric drug delivery systems, Adv. Drug Deliv. Rev. 48 (2–3) (2001) 229–247, https://doi.org/10.1016/S0169-409X(01)00116-8.
[46] P.I. Lee, Modeling of drug release from matrix systems involving moving boundaries: approximate analytical solutions, Int. J. Pharm. 418 (1) (2011) 18–27, https://doi.org/10.1016/j.ijpharm.2011.01.019.
[47] A. Hadjitheodorou, G. Kalosakas, Analytical and numerical study of diffusion-controlled drug release from composite spherical matrices, Mater. Sci. Eng., C 42 (2014) 681–690, https://doi.org/10.1016/j.msec.2014.06.009.
[48] J. Siepmann, F. Siepmann, Modeling of diffusion controlled drug delivery, J. Control. Release 161 (2) (2012) 351–362, https://doi.org/10.1016/j.jconrel.2011.10.006.
[49] P. da Wilton, I. Silva, C.M.D.P.S. Hamawand, e Silva. A liquid diffusion model to describe drying of whole bananas using boundary-fitted coordinates, J. Food Eng. 137 (2014) 32–38, https://doi.org/10.1016/j.jfoodeng.2014.03.029.
[50] P. Wilton, C.M.D.P.S. da Silva, D.D.P.S. e Silva, G. de Silva, Araújo Neves, G.B. Antonio, de Lima, Mass and heat transfer study in solids of revolution via numerical simulations using finite volume method and generalized coordinates for the Cauchy boundary condition, Int. J. Heat Mass Transf. 53 2010, pp. 1183–1194, , https://doi.org/10.1016/j.ijheatmasstransfer.2009.10.028.